Acta Geotechnica (2020) 15:671–680
https://doi.org/10.1007/s11440-019-00768-z

RESEARCH PAPER

Granular hyperelasticity with inherent and stress-induced anisotropy

Yang Xiao[1,2] · Zhichao Zhang[1,2] · Jingkai Wang[1,2]

Received: 23 January 2018 / Accepted: 30 January 2019 / Published online: 8 February 2019

Abstract
A hyperelasticity for granular medium is proposed in this study, considering the inherent and stress-induced anisotropy. The nonlinear elastic behavior is described by defining an elastic potential energy model in terms of the elastic strain invariants that are coupled with a fabric tensor accounting for the transverse isotropy of granular solids formed under gravity. Such an approach provides a unified consideration on the stress-induced and inherent anisotropic behavior of the nonlinear elasticity and its stability. The six independent constants of the elastic modulus tensor of granular medium consolidated under different stress levels and consolidation stress ratios are well predicted using the granular hyperelasticity. Furthermore, the proposed anisotropic model of elastic potential results in a state region within which the thermodynamic stability is broken and thus naturally enables the predictions of the mechanically instable behavior of transversely anisotropic granular solids. From such a thermodynamic perspective, the state boundary of granular medium corresponds to the states at which the positive definiteness of the Hessian matrix of the elastic potential density function is violated and is used to define the strength criterion. Therefore, the proposed granular hyperelasticity in this study provided a generalized approach predicting the nonlinear elasticity and strength criterion of granular medium.

Keywords Granular geomaterials · Hyperelasticity · Inherent anisotropy · Stress-induced anisotropy

1 Introduction

Although had been studied widely from both experimental and numerical perspectives, the understanding of the mechanical behavior of granular materials remains challenging for researchers in the fields of geotechnical engineering. For example, even under static states, the static stress distribution is still a topic of some debate for granular solids [12, 16]. The elastic and plastic behavior of granular solids like sands is heavily dependent on many factors such as the stress state, the porosity and the soil fabric [21, 22, 30]. Especially, the stiffness and strength of granular soils with heterogeneous stress distributions in engineering fields (e.g., foundations and slopes) significantly vary with both the principal stress direction and the inherent anisotropy of soil. DEM simulations for granular materials also show significant evolutions of soil fabric and force chain networks along the imposed stress paths [20]. Therefore, a state- and fabric-dependent constitutive model for granular soils, considering the above-mentioned granular solid behavior, is required for the reasonable predictions of mechanical problems in geotechnical engineering. Anisotropic constitutive relations for sands or clays are usually developed based on extensions to existing models in order to taking into account the effect of anisotropy on the elasto–viscoplastic behavior of soils [1, 5, 11, 23]. In these models, the inherent anisotropy is usually described by the concept of soil fabric tensor. Anisotropic models based on micromechanics considering microstructure and thermodynamics are also studied recently [3, 29], which shows remarkable effects of inherent anisotropy on the cyclic and instability behavior of granular solids.

In most exiting models, the elastic behavior and the strength criterion are in fact usually considered as two independent aspects of soil behavior and thus are separately described by almost different approaches. However,

✉ Zhichao Zhang
zhangzhichaopt@163.com

[1] School of Civil Engineering, Chongqing University, Chongqing 400045, China

[2] Key Laboratory of New Technology for Construction of Cities in Mountain Area (Chongqing University), Ministry of Education, Chongqing 400045, China

from the mechanical and physical perspectives, it can be found that both the elastic stiffness and strength of granular soils are associated with a unified nonlinear elastic regime with a conditional stability of the stress states, which provides an alternative approach giving an insight into the physical mechanisms underlying the granular soil behavior and coupling the state- and fabric-dependent properties of elastic stiffness and strength criterion with each other. A physically reasonable approach accounting for such an elastic regime is the hyperelasticity in which the elastic constitutive relation is derived from an appropriate scalar elastic potential energy or free energy [4, 10, 13, 16]. Such an approach had been studied widely and was also coupled with the plastic behavior of granular solids [15, 27]. The state-dependent behavior as well as the physical meanings behind the elastic stability behavior can be well accounted for within the hyperelastic framework. One of such hyperelastic models for granular solids is the granular elastic model [16], which takes into account the nonlinear elastic stress–strain relation with a mechanically instable region in the static stress space. In this model, the free energy F defined in their hyperelastic model has a functional form as

$$F = A\left(\varepsilon_v^e\right)^m \left[\left(\varepsilon_v^e\right)^2 + \xi\left(\varepsilon_s^e\right)^2\right] \tag{1}$$

with two elastic constants, A (units of stress) and ξ (dimensionless). ε_v^e and ε_s^e are, respectively, the first and second invariants of the elastic strain tensor ε_{ij}^e, defined as

$$\varepsilon_v^e = \varepsilon_{kk}^e, \quad \varepsilon_s^e = \sqrt{e_{ij}^e e_{ij}^e} \tag{2}$$

where $e_{ij}^e = \varepsilon_{ij}^e - \varepsilon_v^e \delta_{ij}/3$ is the deviatoric elastic strain tensor. Here, ε_v^e is also the volumetric elastic strain. Equation (1) gives power law functions of elastic moduli that vary with the mean stress and vanish under stress-free states, and it is just consistent with "Hertz contacts" theory when taking the parameter $m = 1/2$ [7]. Other hyperelastic models had also been proposed by different researches, e.g., the model proposed by Einav and Puzrin [9] and the model by Houlsby [14]. The granular elasticity was also extended to the cohesive materials like silty soils and clays [26, 28].

However, the anisotropy behavior of granular solids, another important aspect of the granular elastic regime that should be coupled with the elastic behavior introduced above, has not been adequately discussed under the physical framework of granular elasticity. In fact, all natural or man-made soil structures, formed under a gravitational field, are transversely isotropic on the bedding plane, with an anisotropic soil fabric [2, 24]. All the mechanical features of soil behavior, including the static, dynamics or quasi-static behavior, could be affected by such inherent anisotropic soil structures. Furthermore, even for the granular materials with an isotropic structure, the so-called stress-induced anisotropy can also be induced by the shearing loads [30]. The objective of this work is to propose a granular hyperelasticity taking both the inherent and stress-induced anisotropy into account. A fabric tensor is incorporated into the free energy function of granular solid to quantify the effects of anisotropy on the elastic moduli, the stress–strain relation and the elastic stability. Consequently, the granular free energy is decomposed into a standard isotropic formula and an anisotropic contribution. A more generalized granular elasticity can be then developed, allowing more accurate interpretations and predictions of the granular elastic behavior, which should be also an important basis of the further studies on granular plasticity. In contrast to other existing nonlinear elastic models developed within the framework of Cauchy elasticity (e.g., the Duncan–Chang model [8]), the approach proposed in this paper describes the state-dependent stress-induced and inherent anisotropy of granular elasticity within a unified energy-based framework in which the thermodynamic laws can always be guaranteed and the anisotropic elastic instability of granular solids can be theoretically determined from the perspective of thermodynamic stability. It has been also shown that such an approach has advantages in giving more comprehensive predictions of granular elastic behavior, comparing with other existing hyperelastic models [25].

2 Theory development

2.1 Fabric tensor of granular solids

The fabric tensor is a concept broadly defined to describe the fabric intensity and orientation of various solids and to relate their macroscopic anisotropy behavior to the microstructures [18, 19, 24]. From the perspective of continuum mechanics and thermodynamics, the effects of inherent anisotropy in granular medium on the stored elastic potential or free energy should depend on such a fabric tensor. In this study, the fabric tensor, represented in the form of second-order symmetric tensor and associated with the orientation distribution of particle contacts [11], will be incorporated into the free energy function of granular solids. Such a kind of fabric descriptor could evolve remarkably toward coaxiality with the stress tensor, following with the so-called stress-induced anisotropy. In this section, only the inherent fabric tensor is discussed and the stress-induced anisotropy will be considered in Sect. 3. In a representative volume of granular media, denoting the

unit normal vector of the αth particle contact plane as u_i^α, the fabric tensor F_{ij} can be then defined as [11]

$$F_{ij} = \frac{3}{N}\sum_{\alpha=1}^{N} u_i^\alpha u_j^\alpha \tag{3}$$

where N is the particle contact number in the representative volume and the subscript α here is not a dummy index. Obviously, the trace of F_{ij} equals 3, i.e., $F_{kk} = 3$.

Commonly formed by a natural deposition process under gravity, the granular medium can be referred to as transversely isotropic materials. At this case, the fabric tensor can have the following simplified matrix form with an inherent anisotropy parameter a:

$$[F_{ij}] = \begin{bmatrix} 1+a & 0 & 0 \\ 0 & 1-\frac{a}{2} & 0 \\ 0 & 0 & 1-\frac{a}{2} \end{bmatrix} \tag{4}$$

Equation (4) is defined in a coordinate system as shown in Fig. 1, in which the "1" is the vertical axis of gravity and the "2" and "3" are the two orthotropic axes on the bedding plane. These three axes constitute the axes of anisotropy. It should be noted that $[F_{ij}]$ can also be redefined with more than one anisotropy parameter in order to describe more generalized anisotropy properties of solids, while only the transverse isotropy is considered in this study. Although the parameter a can have a micromechanical definition, its value can be determined according to the macroscopic observations on its effects on the mechanical properties, e.g., the elastic modulus.

Once the fabric tensor is defined, the orientation distribution of the particle contacts as well as the elastic modulus can be quantified by a distribution function $\rho(\phi,\beta) = F_{ij}n_i n_j$, where $\boldsymbol{n} = \{\cos\phi, \sin\phi\cos\beta, \sin\phi\sin\beta\}$ is the unit direction vector by means of Eulerian angles $\phi \in [0, 2\pi]$ and $\beta \in [0, 2\pi]$ in the local coordinate at interparticle contact as shown in Fig. 1. From Eq. (4), ρ is

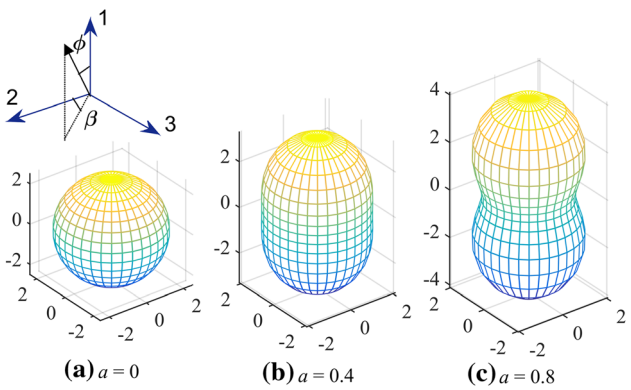

Fig. 1 Schematic plot of orientation distribution of inherent anisotropy of particle contact

independent on β for the case of transverse isotropy. This reads

$$\rho(\phi) = 1 + \frac{a}{4}(3\cos 2\phi + 1) \tag{5}$$

Obviously, the parameters a determine the extent of the anisotropy of granular medium. Figure 1 shows the orientation distribution function defined by Eq. (5) in spherical coordinate. It is obvious that the isotropy just corresponds to the case when $a = 0$. The increase in a leads to a peanut-shaped distribution figuration of the particle contacts, which means more particles contacts and thus larger elastic modulus in the vertical direction. Therefore, using the definition of fabric tensor, the effects of inherent anisotropy on the hyperelasticity of granular medium can be described, as will be discussed below.

2.2 Free energy of anisotropic granular medium

It is assumed here that the free energy of granular medium can be split into different contributions from the isotropy, the stress-induced anisotropy and the inherent anisotropy. The free energy of completely isotropic granular medium had been shown in Eq. (1). Similarly, the granular free energy considering inherent and stress-induced anisotropy can be defined as a function of the invariants of the contraction of the elastic strain tensor and the fabric tensor. As a result, the free energy function will be divided into a pure isotropic part F_{iso}, a stress-induced anisotropic part F_{sa} and an inherent anisotropic part F_{ia}, i.e.,

$$F = F_{\text{iso}} + F_{\text{sa}} + F_{\text{ia}} \tag{6}$$

where F_{iso} is just the free energy function defined in Eq. (1) and therefore

$$F_{\text{iso}} = A\left(\varepsilon_v^e\right)^m \left[\left(\varepsilon_v^e\right)^2 + \xi\left(\varepsilon_s^e\right)^2\right] \tag{7}$$

On the other hand, the contribution of stress-induced anisotropy to the free energy depends on the third invariant of the elastic strain, denoted as ε_t^e, which results in a stress-path-sensitive free energy or elastic properties. If without the effects of inherent anisotropy, F_{iso} together with F_{sa} describes the granular elasticity with initial isotropy. Due to the reasons that will be clear in Sect. 3, we define

$$F_{\text{sa}} = A\left(\varepsilon_v^e\right)^m \zeta \frac{\left(\varepsilon_t^e\right)^5}{\left(\varepsilon_s^e\right)^3}, \quad \varepsilon_t^e = \sqrt[3]{e_{ij}^e e_{jk}^e e_{ki}^e} \tag{8}$$

where ζ is a dimensionless constant quantify the effect of stress-induced anisotropy.

The contribution of inherent anisotropy to the free energy, F_{ia}, must be related to both the elastic strain tensor and the fabric tensor. Noting that the fabric tensor in Eq. (4) is defined in the orthogonal coordinate system

constituted by the axes of anisotropy, a more generalized fabric tensor considering the rotation of coordinate axes should be used here. Without loss of generality, the axis "2" in Fig. 1 is fixed, while the other two axes rotate an angle of θ around the axis "2". The fabric tensor in the new coordinate system, denoted as S_{ij}, can be then specified as

$$[S_{ij}] = [L][F_{ij}][L]^T \tag{9a}$$

$$[L] = \begin{bmatrix} \cos\theta & 0 & \sin\theta \\ 0 & 1 & 0 \\ \sin\theta & 0 & \cos\theta \end{bmatrix} \tag{9b}$$

In order to consider the effects of inherent anisotropy on the granular hyperelasticity, a fabric-related elastic strain tensor, denoted as E_{ij}, is then defined as follows:

$$E_{ij} = \frac{1}{2}\left(\varepsilon^e_{ik}S_{kj} + S_{ik}\varepsilon^e_{kj}\right) \tag{10}$$

Then, F_{ia} can be defined as a function of the invariants of E_{ij} similar to the definition of F_{iso}. This reads

$$F_{\mathrm{ia}} = B\left(\varepsilon^e_v\right)^m\left[\left(E^e_v\right)^2 + \xi_2\left(E^e_s\right)^2\right] \tag{11a}$$

$$E^e_v = E^e_{kk}, \quad E^e_s = \sqrt{\epsilon^e_{ij}\epsilon^e_{ij}} \tag{11b}$$

where E^e_v and E^e_s are the first and second invariants of E_{ij}, B is a material constant with stress dimension and $\epsilon^e_{ij} = E^e_{ij} - E^e_v\delta_{ij}/3$. Noting that Eq. (11a) can be reduced to the isotropic model when taking $a = 0$, the inherent anisotropic free energy described in Eqs. (11a, 11b) is coupled with the isotropic free energy. It is obvious that such a free energy function defined using the fabric-related elastic strain can naturally couple the inherent anisotropy with the conditionally stable nonlinear hyperelasticity of granular solids (see below). Therefore, the elastic behavior of the granular medium in reality can be better reproduced by the model.

The effects of anisotropy on the elastic behavior of granular solids can be studied by free energy isolines in the principal elastic strain space where the coordinate axes $1 \sim 3$ are exactly the anisotropy axes shown in Fig. 1. ε^e_{11}, ε^e_{22} and ε^e_{33} are the three corresponding principal elastic strains. Defining $b = \left(\varepsilon^e_{22} - \varepsilon^e_{33}\right)/\left(\varepsilon^e_{11} - \varepsilon^e_{33}\right)$ as the coefficient of intermediate principal elastic strain and neglecting the stress-induced anisotropy (i.e., $\zeta = 0$), Fig. 1 shows the isolines of free energy, determined by Eqs. (6–8 and 11a, 11b), in the $\varepsilon^e_{11} - \varepsilon^e_{33}$ space. It is obvious that the free energy isolines are bounded by the state line $\varepsilon^e_v = 0$ (or $F = 0$), which indicates the fact that any tensile strain or stress states are impossible for granular medium. For the isotropic cases (Fig. 1a, c), the free energy isolines are relatively uniformly distributed and are symmetric with respect to a line perpendicular to the line $\varepsilon^e_v = 0$. Moreover, the inherent anisotropy results in the significantly asymmetric free energy isolines in the $\varepsilon^e_1 - \varepsilon^e_3$ space, indicating the anisotropic elastic moduli of granular medium. Moreover, it will be clear below that a stable elastic region (SER) and an instable elastic region (IER) can be recognized in Fig. 2 according to the convexity of the free energy isolines, which is also affected by the inherent anisotropy. Similar conclusions can be made for the free energy considering the stress-induced anisotropy. Here, SER and IER are defined as the state regions in which the stability of thermodynamic equilibrium is guaranteed and broken (see Sect. 3.2), respectively.

2.3 Granular hyperelastic relationship

Once the free energy function is defined, the relationship between the stress and the (anisotropy-related) elastic strain can be determined according to the hyperelastic state relation,

$$\sigma_{ij} = \frac{\partial F}{\partial \varepsilon^e_{ij}} \tag{12}$$

Substituting Eqs. (6–8 and 11a, 11b) into Eq. (12) results in

$$\sigma_{ij} = \sigma^{(0)}_{ij} + \sigma^{(ia)}_{ij} \tag{13}$$

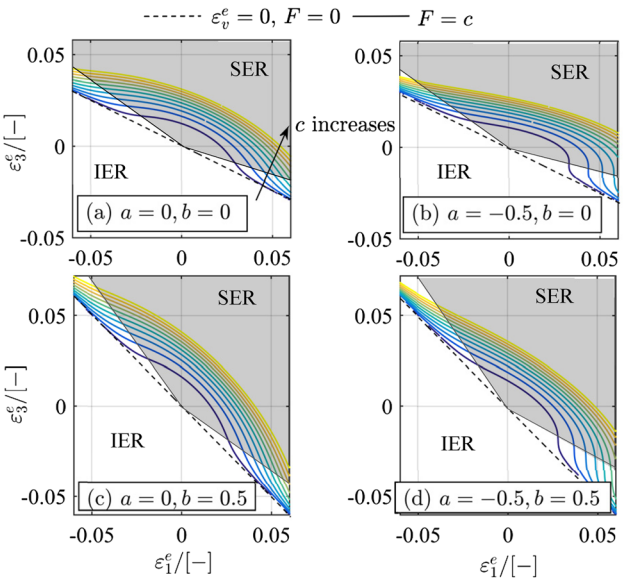

Fig. 2 Isolines of free energy of granular medium in the $\varepsilon^e_1 - \varepsilon^e_3$ space: $A = 0.8$GPa, $B = 8$GPa, $\xi = 0.5$, $\xi_2 = 4$ and $m = 0.5$

$$\sigma_{ij}^{(0)} = A\left(\varepsilon_v^e\right)^{m-1}\left[(m+2)\left(\varepsilon_v^e\right)^2+\xi m\left(\varepsilon_s^e\right)^2+\zeta m\frac{\left(\varepsilon_t^e\right)^5}{\left(\varepsilon_s^e\right)^3}\right]\delta_{ij} + 2A\left(\varepsilon_v^e\right)^m\left[\xi-\frac{3}{2}\zeta\frac{\left(\varepsilon_t^e\right)^5}{\left(\varepsilon_s^e\right)^5}\right]e_{ij}^e + \frac{5}{3}A\left(\varepsilon_v^e\right)^m\zeta\frac{\left(\varepsilon_t^e\right)^2}{\left(\varepsilon_s^e\right)^3}\left[3e_{ik}^e e_{kj}^e-\left(\varepsilon_s^e\right)^2\delta_{ij}\right] \tag{14}$$

$$\sigma_{ij}^{(ia)} = Bm\left(\varepsilon_v^e\right)^{m-1}\left[\left(E_v^e\right)^2+\xi_2\left(E_s^e\right)^2\right]\delta_{ij} + 2B\left(\varepsilon_v^e\right)^m E_v^e S_{ij} + 2B\xi_2\left(\varepsilon_v^e\right)^m \left[\left(E_{in}^e S_{jn}+E_{jn}^e S_{in}\right)/2 - E_v^e S_{ij}/3\right] \tag{15}$$

where $\sigma_{ij}^{(0)}$ and $\sigma_{ij}^{(ia)}$ are the stress parts corresponding to the isotropy/stress-induced anisotropy and to the inherent anisotropy, respectively.

Then, the hyperelastic properties of granular medium, such as the pressure-dependent stress–strain relation and the elastic stability, can be determined by Eq. (15) and coupled with the anisotropy. Detailed discussion will be made in Sect. 3.

3 Discussion on granular elasticity with anisotropy

For granular solids, the elasticity should be state dependent, and a mechanically instable state region should be accounted for in order to interpret the yielding or plastic flowing behavior of granular medium. In this section, the effects of inherent and stress-induced anisotropy on the elastic behavior of granular medium are analyzed according to the granular hyperelasticity developed above.

3.1 Effects of anisotropy on elastic moduli

The anisotropy of granular medium can be checked by analyzing its effects on the elastic moduli and thus on the elastic stress–strain relationship. We first study the following two simple cases.

Case (1) The stresses induced by isotropic elastic straining, i.e., the elastic strain tensor, is diagonal with the three principle elastic strains $\varepsilon_{11}^e = \varepsilon_{22}^e = \varepsilon_{33}^e = \varepsilon^e$. In this case, $\varepsilon_s^e = \varepsilon_t^e = 0$ and thus, the stress-induced anisotropy disappears (see Eq. (8)). However, the inherent anisotropy leads to the three anisotropic principal stresses. Taking $\theta = 0°$ (Eq. 9b) and $a \neq 0$, $\sigma_{11} \neq \sigma_{22} = \sigma_{33}$, as shown in Fig. 3. A larger value of parameter a corresponds to a more significant inherent anisotropy, which can be interpreted by the variation of σ_{33}/σ_{11} with a in Fig. 3.

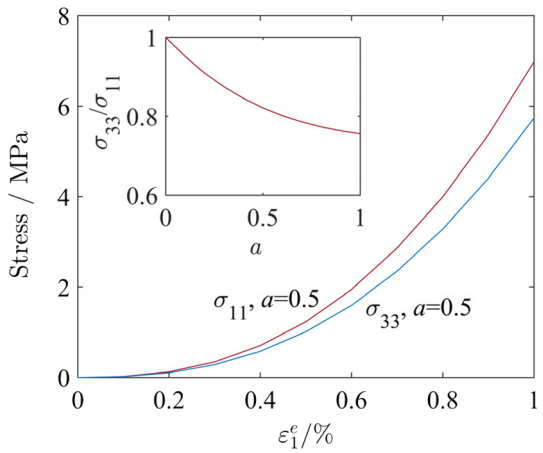

Fig. 3 Stress–strain relations of granular medium subjected to elastic isotropic straining (The parameters used are the same as those used in Fig. 2)

Case (2) The triaxial straining with a constant strain Lode angle ψ is defined as $\cos 3\psi = \sqrt{6}\left(\varepsilon_t^e\right)^3/\left(\varepsilon_s^e\right)^3$, only considering the stress-induced anisotropy (take $B = 0$). The coefficient of intermediate principal elastic strain, b, can also be expressed as a function of ψ, $2b = \sqrt{3}\tan\left(\psi - \frac{\pi}{6}\right) + 1$. As two simple cases, $\psi = 0°$ for the triaxial compression ($b = 0$) and $\psi = 60°$ for the triaxial extension ($b = 1$). From Eq. (14), the deviatoric stress (or shear stress) $\sigma_{11} - \sigma_{33} = 2A\left(\varepsilon_v^e\right)^m[\xi + (\cos 3\psi)^{5/3}\cdot 6^{-5/6}\zeta]\left(\varepsilon_{11}^e - \varepsilon_{33}^e\right)$. Obviously, the shear modulus of granular solids subjected to triaxial compression ($\varepsilon_{11}^e - \varepsilon_{33}^e > 0$ and $\cos 3\psi = 1$) is larger than that of granular solids subjected to triaxial extension ($\varepsilon_{11}^e - \varepsilon_{33}^e < 0$ and $\cos 3\psi = -1$), and the ratio of the former to the latter is $\left(\xi + 6^{-5/6}\zeta\right)/\left(\xi - 6^{-5/6}\zeta\right) > 1$. For the loading paths with values of ψ varying form 0° to 60°, the shear modulus will vary continuously. This is an important stress-induced anisotropic behavior observed in sands, corresponding to the elastic potential defined in Eq. (8). It will be clear that such an elastic potential function also gives the stress-induced anisotropic behavior of mechanical instability, from the energy perspective.

More generally, taking both the inherent and stress-induced anisotropy into account, the elastic behavior can be described by the incremental stress–strain relation,

$$d\sigma_{ij} = c_{ijkl}d\varepsilon_{kl}^e, \quad c_{ijkl} = \frac{\partial^2 F}{\partial\varepsilon_{ij}^e\partial\varepsilon_{kl}^e} = \frac{\partial\sigma_{ij}}{\partial\varepsilon_{kl}^e} \tag{16a – b}$$

where c_{ijkl} is just the tangent elastic modulus tensor. The expression of c_{ijkl} with regard to the (anisotropy-related) elastic strain can be derived by substituting Eqs. (13)–(15) into Eq. (16b) and is not presented here. Since the

anisotropy is considered, the parameter identification becomes undirect, which needs optimization-based inverse analysis from practical point of view [17]. Here, the parameters involved include the two stress-dimensional constants A and B, the two shear modulus coefficient ξ and ξ_2, the stress-induced anisotropy parameter ζ, the inherent anisotropy parameter a and the nonlinearity-related power m. From Eqs. (13)–(15), the elastic modulus of sands has a power functional relationship with the mean stress p with an approximate power of $m/(m+1)$, which can be used to determine the value of m. The value of a can be approximately determined by the ratio between the horizontal and vertical compressive moduli which depend on the contact distribution in different directions (Eq. 15) and can be estimated to be $\rho(90°)/\rho(0°) = (1-a/2)/(1+a)$. Parameters A, B, ξ, ξ_2 and ζ can be then optimized according to the measured compressive and shear moduli on different planes at a certain stress state.

The anisotropic elastic modulus tensor of Ticino river sand (TS), a predominantly silica sand, had been measured by a comprehensive series of laboratory seismic compression and shear wave propagation tests [2]. The tests were carried out under different stress levels and consolidation stress ratio, defined as $K = \sigma'_h/\sigma'_v$ where σ'_h and σ'_v are the effective horizontal and vertical stresses, respectively. As a transversely isotropic material formed under gravity, the vertical direction is just the axis of symmetry and thus, the coordinate system can be defined as the same as the one in Fig. 1. Therefore, in Eq. (9b), $\theta = 0°$. The compressive and shear elastic moduli on different planes can be determined according to the measured wave velocity data. Detailed information can be found in Bellotti (1996) [2]. The hyperelasticity developed here can well predict the anisotropy observed in TS, which heavily depends on the stress path and the stress state. The predicted results are shown in Fig. 4, in which $M_h = C_{2222} = C_{3333}$ and $M_v = C_{1111}$ are the horizontal and vertical compressive moduli, respectively. $G_{hh} = C_{1212}$ is the shear modulus on the plane of isotropy, and $G_{vh} = C_{2323} = C_{3131}$ is the shear modulus on the plane including the axis of symmetry. The measured data of moduli in the case of K = 1 (p = 50 kPa) are used for model calibration.

As shown in Fig. 4, the variations of elastic moduli with the mean stress under different K values are well predicted and are consistent with the laboratory measured data. It is known that the isotropic granular hyperelasticity in Eq. (1) gives K_e $(G_e) \propto p^{m/(m+1)}$, where K_e and G_e are, respectively, the elastic bulk and shear moduli of isotropic materials and p is the mean stress. Similarly, the six independent components of the elastic modulus tensor (Eq. (16b)) are also a power function of the mean stress, but with different powers slightly deviating from

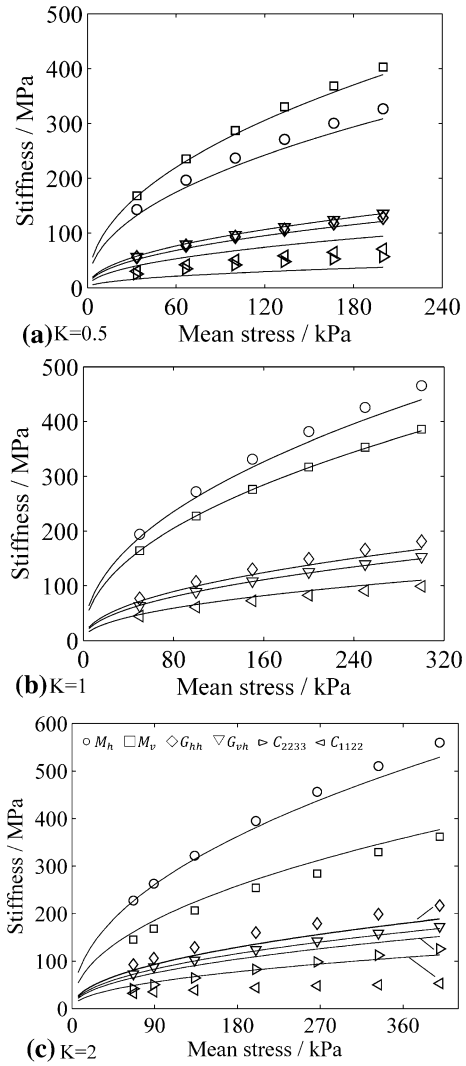

Fig. 4 The compressive and shear moduli of Ticino river sand under different mean stress levels (the solid lines are predicted results and the markers are measured data from [2]: $A = 0.8$GPa, $B = 8$GPa, $a = -0.15$, $\xi = 0.5$, $\xi_2 = 4$, $\zeta = 20$ and $m = 0.9$)

$m/(m+1)$, dependent on the K value. For instance, the power values of the relationships shown in Fig. 4 vary from 0.47 to 0.5, with the parameter m = 0.9. Figure 5 shows the effects of horizontal and vertical stresses on the two constrained moduli. Obviously, the horizontal and vertical constrained moduli are mainly dependent only on the horizontal and vertical stresses, respectively. However, relatively slight variations of the constrained moduli with another stress component are also well predicted.

As shown in Fig. 5, the anisotropy of the modulus tensor is also sensitively dependent on the K value. This can also be interpreted by checking the components of modulus tensor in different rotated coordinate systems. The modulus distribution curves can be then determined as a function of the rotation angle θ, as shown in Fig. 6. The results are well consistent with the measured compressive and shear

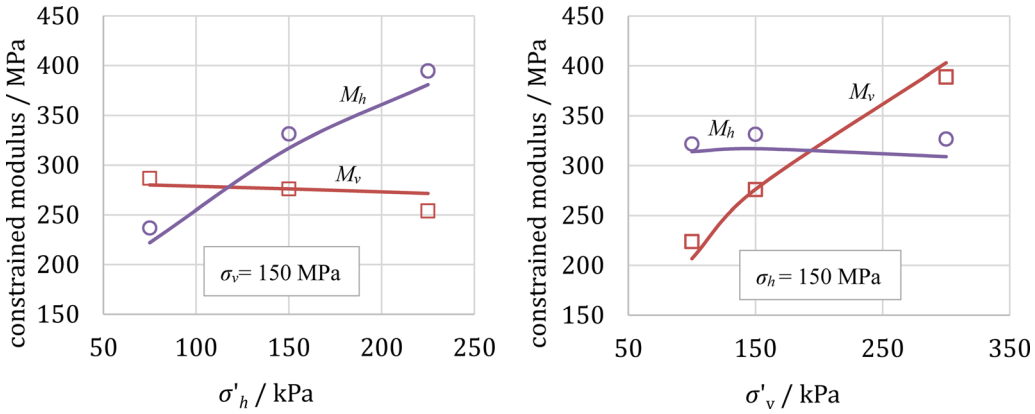

Fig. 5 Effects of **a** horizontal and **b** vertical stresses on the constrained modulus (the dots are measured data [2])

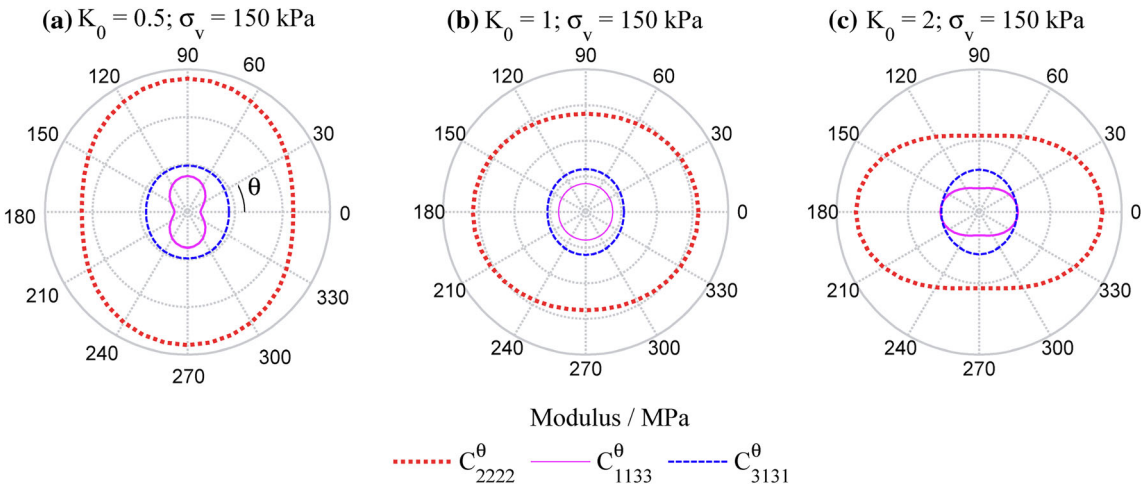

Fig. 6 Elastic moduli calculated in different rotated coordinate systems (θ is the angle of which the axes "1" and "3" are rotated around the axis "2"; parameters are the same as those used in Fig. 4)

wave velocities in different directions [2]. The elliptic or peanut-shaped shape of the modulus surfaces in Fig. 6a, c shows the combined effects of inherent and stress-induced anisotropy. In contrast, the anisotropy shown in Fig. 6b ($K = 1$) is mainly attributed to the inherent anisotropy, since that under isotropic stresses only the isotropy can be observed if no inherent anisotropy exists. Comparing Fig. 6b with Fig. 6a, c, it can be inferred that the stress-induced anisotropy may become dominant for the granular medium consolidated under $K \neq 1$. However, it should be noted that for the transversely isotropic granular medium, the stress-induced anisotropy and the inherent anisotropy should be coupled with each other. Even for $K = 1$, the inherent anisotropy will lead to an anisotropic elastic deformation, resulting in $\varepsilon_t^e \neq 0$ which indicates an additional stress-induced anisotropy described in Eq. (8). Different from Eq. (8), the stress-induced anisotropy is also usually defined as a function of the third invariant of the stress tensor. Such a kind of description of stress-induced anisotropy is equivalent to the one described by the elastic strain tensor (Eq. 8) only for the case without inherent anisotropy. Considering the inherent anisotropy, when $K = 1$, the former type of stress-induced anisotropy will completely disappear, while the latter one can still be observed, as discussed above. Noting that at the particulate scale the particle contact stiffness directly depends on the overlap between particles, a stress-induced anisotropy in terms of the third elastic strain invariant may be more reasonable.

3.2 Effects of anisotropy on strength criterion

For granular solids, there should be a stress state boundary surface beyond which the stress states are impossible to be reached. Such a state boundary can be used to define the strength criterion in the stress space, indicating the ultimate state of the granular solids. From the energy perspective, it will be clear that this state boundary corresponds to the thermodynamic instability of solid materials. For a volume

domain of a solid, denoted as V, the thermodynamic stability requires [6]

$$\delta^2 S = -\frac{1}{T}\int_V \frac{\partial \pi_{ij}}{\partial \varepsilon^e_{kl}} \delta\varepsilon^e_{kl}\delta\varepsilon^e_{ij} \mathrm{d}V \le 0 \tag{17}$$

where T is the temperature, S is the entropy and $\delta^2 S$ is the second variation of entropy. As shown in Fig. 2, the inequality Eq. (17) holds on in the stable elastic region (SER), while is broken in the instable elastic region (IER) that can be associated with the ultimate or failure behavior of granular medium. We can define the state boundary surface as the boundary between SER and IER, which just provides the criterion of granular soils. Noting that Eq. (17) further requires the elastic potential energy density function ω_e be convex with respect to the elastic strain tensor, the state boundary surface just corresponds to the states at which the isolines of the elastic potential energy density are changed from being convex to concave, as illustrated in Fig. 2. In other words, the Hessian matrix $\partial^2\omega_e/\left(\partial\varepsilon^e_{ij}\partial\varepsilon^e_{kl}\right)$, which is also the tangent elastic stiffness matrix, should be positive definite for the stable elastic states of granular solids. Noting that ε^e_{ij} only includes six independent components, the failure surface (or state boundary) in the stress space can be determined according to the critical condition of the positive definiteness of the following matrix:

$$\left[H_{ij}\right] = \frac{\partial^2\omega_e}{\partial X_i \partial X_j} \quad (i,j = 1 \text{ to } 6) \tag{18}$$

where $X_1 = \varepsilon^e_{11}, X_2 = \varepsilon^e_{22}, X_3 = \varepsilon^e_{33}, X_4 = \varepsilon^e_{12}, X_5 = \varepsilon^e_{23}$ and $X_6 = \varepsilon^e_{31}$. Furtherly, the states on the failure line just indicate that $\lambda_{\min} = 0$, where $\lambda_{\min}$ is the minimum eigenvalue of $\left[H_{ij}\right]$.

First, only considering the stress-induced anisotropy under triaxial straining conditions with constant strain Lode angle ψ, as defined in Sect. 3.1, ω_e can be reduced to a function related to the two elastic strain invariants, ε^e_v and ε^e_s. The corresponding strength criterion can be then simply determined by the following relation:

$$\frac{\partial^2\omega_e}{\partial\varepsilon^e_v\partial\varepsilon^e_v}\frac{\partial^2\omega_e}{\partial\varepsilon^e_s\partial\varepsilon^e_s} - \left(\frac{\partial^2\omega_e}{\partial\varepsilon^e_v\partial\varepsilon^e_s}\right)^2 \ge 0 \tag{19}$$

which results in

$$\frac{\varepsilon^e_s}{\varepsilon^e_v} \le \sqrt{\frac{\beta+2}{\beta\left[\xi + (\cos 3\psi)^{\frac{5}{3}}\cdot 6^{-\frac{5}{6}}\zeta\right]}} \tag{20}$$

The state boundary will be reached when Eqs. (19) and (20) become equalities, and the failure can be expected when the above two inequalities are violated. Thus, defining $q = \partial\omega_e/\partial\varepsilon^e_s$ and $p = \partial\omega_e/\partial\varepsilon^e_v$, the strength criterion in the stress space under triaxial conditions can be expressed as:

$$\frac{q}{p} \le \sqrt{\frac{\xi + (\cos 3\psi)^{\frac{5}{3}}\cdot 6^{-\frac{5}{6}}\zeta}{\beta(\beta+2)}} \tag{21}$$

Equation (21) gives the maximum allowable stress ratio q/p dependent on the strain Lode angle. It indicates that the energy part defined in Eq. (8) also determines the effects of stress-induced anisotropy on the strength of granular medium. It is interesting that the elastic potential reveals both the state-dependent nonlinear hyperelastic stress–strain relation and the mechanical instability of granular medium. This makes the model be capable of giving the unified understanding and predictions of different properties of the granular solids behavior, within a minimum complexity. Figure 7a shows the strength criteria in the principal stress space determined using Eq. (21). The

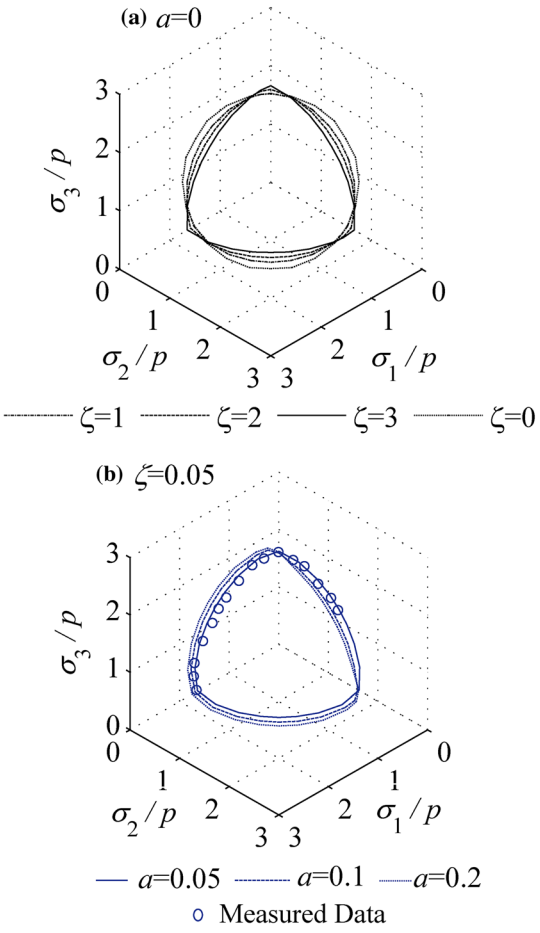

Fig. 7 Strength criteria in the normalized principal stress space **a** only considering the stress-induced anisotropy and **b** considering both the stress-induced and inherent anisotropy. The circles are the measured data for Camber Cambria River Sand [5]. Parameters not mentioned used are the same as those used in Fig. 4

failure surface is changed from a circle to a triangle when the parameter ζ increases from 0 to a larger value, indicating the effect of stress-induced anisotropy.

More generally, when considering both the stress-induced and inherent anisotropy under arbitrary state paths, the states at which the failure is triggered and thus the strength criterion (i.e., the state boundary) can be determined by searching the states where $\lambda_{\min} = 0$ for $[H_{ij}]$, along different specific stress or strain paths (e.g., the searching path with a constant strain Lode angle ψ in the principal elastic strain space, as shown in Fig. 8). Figure 7b shows the calculated strength criteria in a specific principal stress space, with a fixed parameter ζ and different values of a, the parameter of inherent anisotropy. The subscript "1" in Figs. 7 and 8 represents the symmetry axis of transversely isotropic materials, which is just in the vertical direction for the granular medium formed under gravity. Figure 7b indicates that the increased inherent anisotropy parameter a shifts the state boundary to the direction "1", resulting in more significant strength anisotropy. The triaxial compression strength for the cases in which the maximum principal stress is located on the bedding plane, however, seems to be independent on the value of a.

Figure 7 only shows the strength criteria under the triaxial conditions with the three principal stress directions coincide with the axes of anisotropy, while Fig. 9 shows the predicted stress–strain relations under more generalized triaxial compression conditions. θ is the angle between the direction of maximum principal stress (referred to as the axial direction here) and the symmetry axis of transverse isotropy. $\sigma_a^{(\theta)}$ and $\sigma_l^{(\theta)}$ are the axial and lateral stresses, respectively; $J_2 = \sqrt{(\sigma_{ij} - p\delta_{ij}/3)(\sigma_{ij} - p\delta_{ij}/3)}$ is the second invariant of the deviatoric stress tensor. For the triaxial loadings with constant $\sigma_l^{(\theta)}$ and increasing $\sigma_a^{(\theta)}$, the failure is triggered at the peak state in the stress–strain

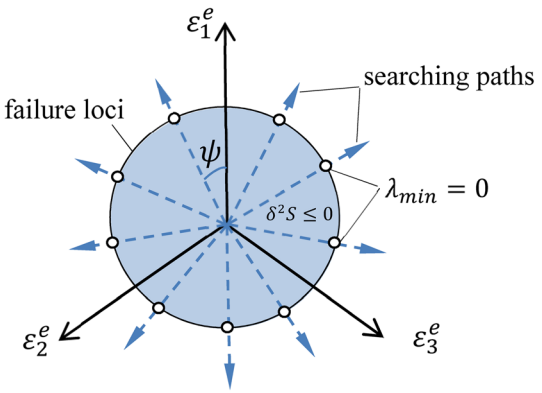

Fig. 8 Schematic diagram of the determination of failure loci in the principal elastic strain space

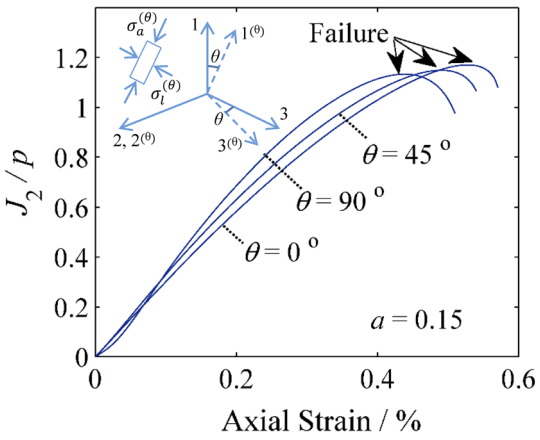

Fig. 9 Effects of principal stress direction on the triaxial compression behavior of anisotropic granular solids

relations shown in Fig. 9. On the whole, with the increase in θ, the stiffness is decreased at a low strain level and increased at a relatively high strain level; however, the peak strength tends to be decreased. Variations presented above in the stiffness and failure states of granular medium are completely attributed to the inherent anisotropy. Such properties are important for the circumstances where the directions of principal stresses vary spatially, e.g., in the slopes.

4 Conclusion

In this paper, the transverse isotropy of granular medium is studied within the energy perspective. Both the stress-induced and inherent anisotropy can be well described by the granular hyperelasticity in which a fabric tensor is coupled to the elastic potential energy density in terms of the elastic strain invariants. The third elastic strain invariant is employed to enable the description of the stress-induced anisotropy. It can be concluded that such an approach provides a unified considerations on the stress-induced and inherent anisotropic behavior of the nonlinear elasticity and its stability. It provides an insight into the physical mechanisms underlying the granular soil behavior and couples the state and fabric-dependent properties of elastic stiffness and strength criterion with each other. The six independent constants of the elastic modulus tensor of granular medium consolidated under different stress levels and consolidation stress ratios are well predicted using the granular hyperelasticity. Furthermore, it is shown that proposed model of elastic potential, coupled with the fabric tensor, results in a state region within which the thermodynamic stability is broken and thus naturally enables the predictions of the state boundary and the mechanical instability of transversely isotropic granular solids.

From such a thermodynamic perspective, the strength criterion or the state boundary, which is usually defined in granular mechanics and should be affected by the stress-induced and inherent anisotropy, can be quantitatively determined by searching the states at which the positive definiteness of the Hessian matrix of the elastic potential density function is violated. The stress-induced anisotropy changes the shape of the strength criterion, while the inherent anisotropy mainly leads to the shifting of the strength criterion in the stress space. Therefore, the proposed granular hyperelasticity in this study provided a generalized approach predicting the nonlinear elasticity and strength criteria of granular medium. It can be expected that such a hyperelasticity could be useful in the further modeling of elasto–plastic granular behavior.

Acknowledgements This study was supported by the National Natural Science Foundation of China (No. 51608072), the Fundamental Research Funds for the Central Universities (No. 106112016CDJXY200006) and the Chongqing Science and Technology Commission (No. cstc2017jcyjAX0061), to which we hereby express our sincere gratitude.

References

1. Andrew JW, Kavvadas MJ (1994) Formulation of MIT-E3 constitutive model for overconsolidated clays. J Geotech Eng 120(1):173–198
2. Bellotti R, Jamiolkowski M, Lo Presti DCF, O'Neill DA (1996) Anisotropy of small strain stiffness in Ticino sand. Geotechnique 46(1):115–131
3. Chang CS, Yin ZY (2010) Micromechanical modeling for inherent anisotropy in granular materials. J Eng Mech 136:830–839
4. Coleman BD, Gurtin ME (1967) Thermodynamics with internal state variables. J Chem Phys 47:597–613
5. Dafalias YF, Papadimitriou AG, Li XS (2004) Sand plasticity model accounting for inherent fabric anisotropy. J Eng Mech 130(11):1319–1333
6. De Groot SR, Mazur P (1962) Non-equilibrium thermodynamics. North-Holland Pub. Co, Amsterdam
7. Duffy J, Mindlin RD (1957) Stress-strain relations and vibrations of a granular medium. J Appl Mech 24:585–593
8. Duncan JM, Chang CY (1970) Nonlinear analysis of stress and strain in soils. J Soil Mech Found Div 96:1629–1652
9. Einav I, Puzrin AM (2004) Pressure-dependent elasticity and energy conservation in elastoplastic models for soils. J Geotech Geoenviron 130(1):81–92
10. Fung YC (1965) Foundation of solid mechanics. Prentice-Hall, New Jersey
11. Gasser TC, Ogden RW, Holzapfel GA (2006) Hyperelastic modelling of arterial layers with distributed collagen fiber orientations. J R Soc Interface 3(6):15
12. Gennes PGD (1999) Granular matter: a tentative view, more things in heaven and Earth. Springer, New York, pp S374–S382
13. Houlsby GT (1985) The use of a variable shear modulus in elastic-plastic models for clays. Comput Geotech 1(1):3–13
14. Houlsby GT (2005) Elastic moduli of soils dependent on pressure: a hyperelastic formulation. Géotechnique 55(5):383–392
15. Houlsby GT, Puzrin AM (2000) A thermomechanical framework for constitutive models for rate-independent dissipative materials. Int J Plas 16(9):1017–1047
16. Humrickhouse PW, Sharpe JP, Corradini ML (2010) Comparison of hyperelastic models for granular materials. Phys Rev E 81(1):011303
17. Jin YF, Yin ZY, Wu ZX et al (2018) Identifying parameters of easily crushable sand and application to offshore pile driving. Ocean Eng 154:416–429
18. Ochia H, Lade PV (1984) Three-dimensional behavior of sand with anisotropic fabric. J Geotech Eng 109(10):1313–1328
19. Schröder J, Neff P, Balzani D (2005) A variational approach for materially stable anisotropic hyperelasticity. Int J Solids Struct 42(15):4352–4371
20. Shi JS, Guo PJ (2018) Fabric evolution of granular materials along imposed stress paths. Acta Geotech 13:1341–1354
21. Xiao Y, Liu H (2017) Elastoplastic constitutive model for rockfill materials considering particle breakage. Int J Geomech 17:04016041
22. Xiao Y, Sun Y, Yin F, Liu H, Xiang J (2017) Constitutive modeling for transparent granular soils. Int J Geomech 17:04016150
23. Yin ZY, Chang CS, Karstunen M et al (2010) An anisotropic elastic–viscoplastic model for soft clays. Int J Solids Struct 47(5):665–677
24. Yin ZY, Chang CS, Hicher PY (2010) Micromechanical modelling for effect of inherent anisotropy on cyclic behaviour of sand. Int J Solids Struct 47(14):1933–1951
25. Zhang ZC (2013) Research on multi-field coupling thermodynamic constitutive theory and model for saturated geomaterials. Tsinghua University
26. Zhang Z (2017) A thermodynamics-based theory for the thermo-poro-mechanical modeling of saturated clay. Int J Plast 92:164–185
27. Zhang Z, Cheng X (2014) Effective stress in saturated soil: a granular solid hydrodynamics approach. Granul Matter 16(5):761–769
28. Zhang Z, Cheng X (2015) A thermodynamic constitutive model for undrained monotonic and cyclic shear behavior of saturated soils. Acta Geotech 10(6):781–796
29. Zhao CF, Yin ZY, Misra A et al (2017) Thermomechanical formulation for micromechanical elasto-plasticity in granular materials. Int J Solids Struct 138:64–75
30. Zhou H, Liu HL, Kong GQ (2018) Influence of stress anisotropy on the cylindrical cavity expansion in undrained elastic-perfectly plastic soil. Sci China Technol Sc 61(3):1–11